BBA - Molecular Basis of Disease 1867 (2021) 166084

Contents lists available at ScienceDirect

BBA - Molecular Basis of Disease

journal homepage: www.elsevier.com/locate/bbadis

Deletion of phospholipase D1 decreases bone mass and increases fat mass via modulation of Runx2, β-catenin-osteoprotegerin, PPAR-γ and C/EBPα signaling axis

Dong Woo Kang [a,b,1], Won Chan Hwang [a,c,1], Yu Na Noh [a], Xiangguo Che [d], Soung-Hoon Lee [e], Younghoon Jang [f], Kang-Yell Choi [e], Je-Yong Choi [d], Do Sik Min [c,*]

[a] Department of Molecular Biology, College of Natural Science, Pusan National University, Busan 609-735, Republic of Korea
[b] Institute for Innovative Cancer Research, Asan Medical Center, University of Ulsan College of Medicine, Seoul, Republic of Korea
[c] College of Pharmacy, Yonsei University, Incheon 21983, Republic of Korea
[d] Department of Biochemistry and Cell Biology, Korea Mouse Phenotyping Center, Cell and Matrix Research Institute, BK21 Plus KNU Biomedical Convergence Program, School of Medicine, Kyungpook National University, Daegu 41944, Republic of Korea
[e] Department of Biotechnology, College of Life Science and Biotechnology, Yonsei University, Seoul, Republic of Korea
[f] Department of Biology and Chemistry, Changwon National University, Changwon, Republic of Korea

ARTICLE INFO

Keywords:
Phospholipase D1
Osteogenesis
Osteoclastogenesis
Bone mass
Adipogenesis
Fat mass

ABSTRACT

In osteoporosis, mesenchymal stem cells (MSCs) prefer to differentiate into adipocytes at the expense of osteoblasts. Although the balance between adipogenesis and osteogenesis has been closely examined, the mechanism of commitment determination switch is unknown. Here we demonstrate that phospholipase D1 (PLD1) plays a key switch in determining the balance between bone and fat mass. Ablation of *Pld1* reduced bone mass but increased fat in mice. Mechanistically, *Pld1*$^{-/-}$ MSCs inhibited osteoblast differentiaion with diminished Runx2 expression, while osteoclast differentiation was accelerated in *Pld1*$^{-/-}$ bone marrow-derived macrophages. *Pld1*$^{-/-}$ osteoblasts showed decreased expression of osteogenic makers. Increased number and resorption activity of osteoclasts in *Pld1*$^{-/-}$ mice were corroborated with upregulation of osteoclastogenic markers. Moreover, *Pld1*$^{-/-}$ osteoblasts reduced β-catenin mediated-osteoprotegerin (OPG) with increased RANKL/OPG ratio which resulted in accelerated osteoclast differentiation. Thus, low bone mass with upregulated osteoclasts could be due to the contribution of both osteoblasts and osteoclasts during bone remodeling. Moreover, ablation of *Pld1* further increased bone loss in ovariectomized mice, suggesting that PLD1 is a negative regulator of osteoclastogenesis. Furthermore, loss of PLD1 increased adipogenesis, body fat mass, and hepatic steatosis along with upregulation of PPAR-γ and C/EBPα. Interestingly, adipocyte-specific *Pld1* transgenic mice rescued the compromised phenotypes of fat mass and adipogenesis in *Pld1* knockout mice. Collectively, PLD1 regulated the bifurcating pathways of mesenchymal cell lineage into increased osteogenesis and decreased adipogenesis, which uncovered a previously unrecognized role of PLD1 in homeostasis between bone and fat mass.

Abbreviations: ALT, alanine aminotransferase; ALP, alkaline phosphatase; Ap2, adipoprotein2; AST, aspartate aminotransferase; BAT, brown adipose tissues; BMMs, bone marrow-derived macrophages; BSP, bone sialoprotein; BS/BV, bone surface/volume ratio; BV/TV, bone volume fraction; Conn. D, connectivity density; C/EBPα, CCAAT enhancer binding protein alpha; Runx2, runt-related transcription factor 2; eWAT, epididymal white adipose tissues; NFATc1, nuclear factor of activated T cells 1; M-CSF, macrophage colony-stimulating factor; MSC, mesenchymal stem cells; OCN, osteocalcin; OPG, osteoprotegerin; OVX, ovariectomy; PLD1, phospholipase D1; PPAR-γ, peroxisome proliferator activated receptor-gamma; pOB, preosteoblasts; qRT-PCR, quantitative real time-polymerase chain reaction; RANKL, receptor activator of nuclear factor kappa-B ligand; SMI, structure model index; SREBP1c, sterol regulatory element binding protein 1c; Tb.N, trabecular number; Tb.Sp, trabecular separation; Tb.Th, trabecular thickness; TG, transgenic; TRAP, tartrate-resistant acid phosphatase; μCT, micro-computed tomography.

* Corresponding author at: College of Pharmacy, Yonsei University, 85 Songdogwahak-ro, Yeonsu-gu, Incheon 21983, Republic of Korea.
E-mail address: minds@yonsei.ac.kr (D.S. Min).

[1] Dong Woo Kang and Won Chan Whang contributed equally to this work.

https://doi.org/10.1016/j.bbadis.2021.166084
Received 8 September 2020; Received in revised form 12 January 2021; Accepted 20 January 2021
Available online 23 January 2021

1. Introduction

Bone marrow-derived multipotent mesenchymal stem cells (MSCs) undergo differentiation into various anchorage-dependent cell types, including osteoblasts and adipocytes [1]. It has been suggested that a reciprocal relationship exists between osteoblasts and adipocytes during the differentiation of MSCs [2,3]. The relationship between bone and fat formation within the bone marrow microenvironment is complex and remains an area of active investigation. Although various cell types can be derived from MSCs, commitment of these cells into adipocytes and osteoblasts is specifically related to the pathological conditions of abnormal bone remodeling [2]. With age, mesenchymal stem cells in the bone marrow become inclined to undergo differentiation into adipocytes rather than osteoblasts, resulting in increased number of adipocytes and decreased number of osteoblasts, causing osteoporosis [2,3]. The deranged balance of these processes causes an elevated risk of fractures with age.

The commitment of MSCs towards either the osteoblast or adipocyte lineages depends on lineage-specific transcriptional regulators. Various transcription factors play as key regulators of adipogenesis and osteogenesis. For example, the nuclear receptor, peroxisome proliferator-activated receptor gamma (PPAR-γ and CCAAT enhancer binding protein α (C/EBPα) are critical regulators of adipogenesis [4] and also function as positive and negative modulators for osteoclastogenesis [5–7] and osteoblastogenesis [8,9], respectively. Runx2 is a master transcription factor for osteoblast differentiation [10–12]. Interestingly, however, PPAR-γ suppresses osteogenesis via inhibition of Runx2 transcriptional activity [13].

Osteoblasts orchestrate osteoclast-mediated bone destruction by expressing M-CSF and receptor activator of NF-κB ligand (RANKL) as well as osteoprotegerin (OPG) [14]. RANKL binds to its receptor RANK on osteoclast precursors to mediate osteoclast differentiation and subsequent activation. OPG, a soluble decoy receptor for RANKL, blocks RANKL binding to RANK and thereby inhibits osteoclast differentiation [15]. Despite the availability of adequate information regarding various regulatory factors in each cell linage pathway, the molecular mechanisms of coordinating the balance between osteogenesis and adipogenesis are still limited. Two isoforms of phospholipase D (PLD), PLD1 and PLD2, hydrolyze phosphatidylcholine, the most abundant membrane phospholipid, to generate choline and the second messenger signaling lipid, phosphatidic acid [16]. PLD isozymes have been implicated in a wide range of pathophysiological processes including proliferation, oncogenesis, inflammation, phagocytosis, and neurodegenerative diseases [17,18]. Although only a few studies have been reported on the involvement of PLD in osteogenesis and osteoclastogenesis [19–22], the function and molecular mechanisms of PLD in bone formation, bone resorption and adipogenesis remain unclear. In this study, we report a role of PLD1 as a key regulator of bone and fat homeostasis through Runx2, β-catenin-OPG, PPAR-γ and C/EBPα axis.

2. Materials and methods

2.1. Materials

Alkaline phosphatase (ALP) kit, silver nitrate, Alizarin Red S, methyl green, toluidine blue, β-glycerophosphate, and ascorbic acid were purchased from Sigma-Aldrich (St. Louis, MO, USA). Dulbecco's Modified Eagle Medium, fetal bovine serum, trypsin-EDTA, and antibiotic-antimycotic solution were purchased from GibcoBRL (Grand Island, NY, USA). The polyclonal anti-PLD antibody, that recognizes both PLD1 and PLD2, was generated as described previously [23]. Runx2, TAZ, PPAR-γ, C/EBPα, and SREBP1 antibodies were purchased from Cell Signaling Inc. (Danvers, MA, USA). Antibody to OPG was from Abcam (Cambridge, UK). Horseradish peroxidase-conjugated antibodies to rabbit IgG or mouse IgG were purchased from Kirkegaard & Perry, Inc. (Gaithersburg, MD, USA).

2.2. Plasmids and small interfering RNA

Wild type PLD1 (WT-PLD1) construct was cloned into the *Apa*I site of the pLVX-ZsGreen1-lentiviral plasmid (Clontech). The promoter constructs of pGL3-Runx2-P1 (4.7 kb), pGL3-ALP (0.6 kb), pGL3-OCN (0.8 kb), and pGL3-BSP (0.4 kb) were used for transient transfection assays as described in a previous study [3]. A stable β-catenin mutant (S37A β-catenin) was used. pcDNA3 PPAR-γ2 and the promoters for pGL3-PPAR-γ and pGL3-aP2 were kindly provided by Dr. J Cheong (Pusan National University, Busan, Republic of Korea). The TAZ promoter (−3550/+483) was amplified from human genomic DNA and cloned into pGL4.14b luciferase reporter plasmid (Promega, Madison, WI, USA). A scrambled sequence was used as a control for off target effects of shRNA. The shRNA sequences were as follows: shPLD1-a (1571–1591): AAGGUGGGACGACAAUGAG, shPLD1-b (4975–3051): AGGACAUUCAGGAUCCAGUGA, shScramble: GCGCGCTTTGTAGGATTCG. The sequences were cloned into a pLKO1-lentiviral plasmid (Sigma-Aldrich). RUNX2 shRNA (iLenti-GFP shRUNX2 vector, i000153) and its control vector (iLenti-GFP, LV015G) were purchased from Abmgood (Richmond, Canada).

2.3. Mice strains

PLD1-deficient C57BL/6 mice (*Pld1*$^{-/-}$) were kindly provided by Dr. Gilbert Di Paolo (Columbia University Medical Center) [24]. To generate adipocyte-specific PLD1 transgenic C57BL/6 mouse (*aP2-GFP-PLD1* Tg mouse, *Pld1*^{Tg}), GFP-PLD1 was inserted downstream of the *aP2* promoter (Macrogen Inc., Korea). *Pld1*$^{-/-}$*Pld1*^{Tg} mice were generated by crossing *Pld1* Tg with *Pld1*$^{-/-}$ mice. All mice were housed at 25 °C under a 12:12 h light/dark cycle. All animal procedures were performed in accordance with the institutional guidelines for animal research and were approved by the Institutional Animal Care Committee of Pusan National University.

2.4. Bone structure analysis

After removing the soft tissues, the femur bone structure of male mice or ovariectomized (OVX) female mice was analyzed using micro-computed tomography (μCT) (GE Healthcare, Little Chalfont, Buckinghamshire, United Kingdom). Scans were obtained using a source voltage of 80 kV and a source current of 80 μA. The resolution was set to 10 μm. Structural parameters for trabecular and cortical bone were analyzed using the built-in software of the μCT. Bone parameters and density were analyzed at the region between 0.7 mm and 2.3 mm below the growth plate of the distal femur. All bone (μCT) nomenclature followed the guidelines of the American Society for Bone and Mineral Research [25]. Total bone mineral density (BMD) was measured, and trabecular parameters were evaluated as the bone volume expressed per unit total volume (BV/TV), trabecular number (Tb.N), trabecular separation (Tb.Sp), trabecular thickness (Tb.Th), and structural model index (SMI). Three-dimensional bone structure image slices were reconstructed using the built-in software.

2.5. Ovariectomy of mice

The ovary from *Pld1*$^{+/+}$ and *Pld1*$^{-/-}$ female mice was resected bilaterally at 12 weeks of age. Briefly, each female mouse was anesthetized with sodium pentobarbital (65 mg kg^{-1}, i.p.) before being placed on its ventral surface without restraint. Following an incision made with a small pair of scissors and forceps, the periovarian fat was grasped, and the ovary was pulled through the opening in the musculature. A ligature was placed around each ovary and fallopian tube before the ovaries and periovarian fat were resected bilaterally. Sham-operated animals underwent the same procedure as the OVX female mice but without resection of the ovaries.

2.6. Alcian blue and Alizarin Red S staining and histological analyses

The tissue was fixed in 95% ethanol for four days, transferred to acetone for three days and subsequently transferred to 0.03% Alcian blue 8GX staining solution (Sigma), 0.015% Alizarin Red S staining solution (Sigma) and 5% glacial acetic acid in ethanol at 37 °C for two days and at room temperature for one more day. Tissue was cleared in 1% potassium hydroxide for several days and then, bone sections were decalcified in 10% formic acid for three weeks, dehydrated in ethanol, and rinsed in xylene. Tissues were then embedded in paraffin and cut into 4 μm sections. The sections were stained with Alcian Blue and Alizarin Red S staining solutions. Images were captured using a DP71 digital camera (Olympus, Center Valley, PA, USA) attached to an Olympus BX41 microscope at 400× magnification [26].

2.7. Culturing of MSCs

Human bone marrow-derived MSCs (hMSCs) were purchased from Cambrex BioScience (Walkersville, MD, USA) and cultured in Dulbecco's Modified Eagle Medium (low glucose) containing 20% fetal bovine serum (FBS) (Invitrogen, NY, USA). MSCs cultured until six passages were used for the experiments. Cells were cultured at 37 °C in a humidified incubator with 5% CO_2. Mouse bone marrow-derived MSCs (mMSCs) were generated from 6 to 8-week old *Pld1*$^{+/+}$ littermates and *Pld1*$^{-/-}$ mice. Bone marrow cells were collected by flushing femurs and tibias with Hank's balanced salt solution (HBSS) and plated at a density of 10^6 cells/cm^2 in murine mesenchymal medium with murine mesenchymal supplements (MesenCult, Stem Cell Technologies, BC, Canada). Nonadherent cells were removed after 24 h, and culture medium was replaced every three days. mMSCs at passage 2 to passage 5 were used in the described experiments.

2.8. In vitro coculture of osteoblast with BMMs

Neonatal murine calvarial cells were prepared as previously described [27,28]. Briefly, calvariae of newborn *Pld1*$^{+/+}$ littermates and *Pld1*$^{-/-}$ mice were dissected and washed twice with 4 mM EDTA in PBS in a 37 °C water bath with shaking. The calvariae were then digested with 20 μg/ml collagenase type II (Worthington Biomedical Corporation, Freehold, NJ) in PBS for 10–15 min each for 5 times. Cells from the last three digestions, which were highly enriched in osteoblastic cells, were collected and used as the starting population of cells [29]. Mouse calvarial cells were cocultured with BMM in α-MEM containing 10% fetal calf serum (CSL Limited, Victoria, Australia) in 48-well plates (CORNING Inc., Corning, NY). All cultures were maintained at 37 °C in a humidified atmosphere of 5% CO_2 in air.

2.9. Osteoblast differentiation assay

Osteoblast differentiation was induced by exposure of confluent MSCs to osteoblast induction medium (OIM; 10% FBS, 0.1 μM dexamethasone, 10 mM β-glycerolphosphate, and 50 μM ascorbic acid in α-minimum essential medium), and extracellular matrix calcification was visualized by Alizarin Red S staining. The osteogenic medium was changed every two days. Briefly, cells were washed twice with PBS and fixed with 95% ethanol at 4 °C for 30 min. Fixed cells were incubated with 4% Alizarin Red-S (Sigma) for 15 min with shaking. To minimize non-specific staining, cells were rinsed five times with deionized water and once with PBS for 20 min. Osteoblast differentiation was quantified by measuring the area of Alizarin Red S staining and images were captured using a digital camera equipped with Nikon TS100 inverted microscope (Nikon, Japan) and 10×/0.25 ph 1 ADL or LWD 40×/0.55 ph 1 ADL, and, the density using Scion imaging software (Scion Corporation, Frederick, MD, USA).

2.10. Adipogenic differentiation assay

MSCs were cultured to confluency in growth medium and then treated with adipogenic induction medium (AIM; 10% FBS, 0.1 μM dexamethasone, 0.5 mM 1-methyl-3-isobutylxanthine, 10 μg/ml insulin, and 200 μM indomethacin). As described previously [30], accumulation of intracellular triglyceride droplets was visualized by Oil Red O (ORO) staining, and phase contrast images were captured using a digital camera equipped with a Nikon inverted microscope (Nikon, Japan) using 10×/0.25 ph 1 ADL or LWD 40×/0.55 ph 1 ADL.

2.11. Osteoclastogenesis assay

Bone marrow cells from mouse were isolated, cultured, and differentiated into osteoclast in the presence of 10% FBS DMEM containing 30 ng/mL of mouse M-CSF (R&D systems) and 50 ng/mL mouse RANKL (R&D systems). The pit formation was performed in BioCoat OSTEOLOGIC™ Bone Cell Culture System plates (BD Biosciences) that had been coated with a thin film of calcium phosphate for 5 d. The cells were removed, and total resorption pits were observed under a bright-field microscope as clear zones in the matrix. The resorbed areas on the plates were captured with a digital camera attached to the microscope and analyzed by a soft imaging system. The percentage of resorption was calculated by considering the area of a single well as 100% with six to eight wells per group. TRAP staining was performed with the aid of a commercial kit (Sigma-Aldrich), according to the manufacturer's instructions. TRAP-positive multinucleated cells containing three or more nuclei were counted as mature osteoclasts. TRAP activity was determined as previously described [31].

2.12. Transient transfections and luciferase reporter assay

MSCs were plated in 12-well plates at 1×10^5 cells/well and grown to 60–70% confluency. Plasmid mixtures containing luciferase reporter plasmids were transfected using Lipofectamine Plus, according to the manufacturer's instructions. Following 24 h of transfection, reporter activity was measured using the dual luciferase assay system (Promega). For transfection efficiency, relative luciferase activity was calculated by normalizing firefly luciferase activity against *Renilla* luciferase activity of the internal control.

2.13. ELISA

Serum from 5-week-old mice ($n = 6$) was isolated, and OPG levels were measured using the Quantikine mouse OPG ELISA kit (R&D systems).

2.14. RNA isolation and quantitative real-time PCR (q-PCR)

Total RNA from cells or bone tissues was isolated using the Trizol reagent (Sigma, St. Louis, MO, USA). First-strand cDNA was synthesized using AMV-RTase (Promega, Madison, WI, USA). Real-time q-PCR was performed with cDNA using the SsoFast EvaGreen qRT-PCR kit (Bio-Rad) and CFX96 Real Time System (Bio-Rad). All data were normalized with GAPDH or β-Actin gene expression values. Oligonucleotide primer sequences are listed in Supplemetary Table 1.

2.15. Statistics

Data are represented as mean ± SEM. Data were analyzed by the Student's *t*-test and ANOVA. Results were considered as statistically significant when $P < 0.05$.

3. Results

3.1. Loss of PLD1 decreases bone mass

We first investigated whether PLD1 regulates bone homeostasis using in vivo *Pld1*$^{-/-}$ male mice. *Pld1*$^{-/-}$ mice showed lower trabecular bone mass than *Pld1*$^{+/+}$ littermates as analyzed by micro-computed tomography (μCT) at 12 weeks of age (Fig. 1A). Bone histomorphometric analysis revealed that the bone volume fraction (BV/TV), trabecular thickness (Tb.Th), trabecular number (Tb.N) and connectivity density (Conn. D), were markedly decreased in *Pld1*$^{-/-}$ mice, compared to that of *Pld1*$^{+/+}$ littermates. However, bone surface/volume ratio (BS/BV), trabecular separation (Tb.Sp), and structure model index (SMI) were significantly increased (Fig. 1B), suggesting weak bone strength in *Pld1*$^{-/-}$ mice. However, there was no significant difference in cortical bone between *Pld1*$^{-/-}$ and *Pld1*$^{+/+}$ mice (Supplementary Fig. 1). Low bone mass of *Pld1*$^{-/-}$ mice may be due to the high activity of osteoclasts. The percentage of bone surface covered by osteoclasts (Oc. S/BS) was significantly increased in *Pld1*$^{-/-}$ mice at 12 or 60 days of age, as analyzed by tartrate-resistant acid phosphatase (TRAP) staining (Fig. 1C and D). Osteoclast number was increased two to three fold in *Pld1*$^{-/-}$ mice compared to wild type (WT) littermate mice (Fig. 1D). Taken together, these results indicate that deletion of PLD1 decreases trabecular bone mass.

3.2. *Pld1*$^{-/-}$ MSCs inhibits osteoblast differentiation

To investigate the role of PLD1 during osteogenesis in vitro, MSCs were differentiate into osteoblasts under osteogenic media. Expression of Runx2 was increased during osteoblast differentiation as shown in Fig. 2a and b. Interestingly, expression of PLD1 but not PLD2, was also increased during osteoblast differentiation (Fig. 2A and B). MSCs derived from *Pld1*$^{-/-}$ mice suppressed osteogenic differentiation as analyzed by Alizarin Red S staining (Fig. 2C). *Pld1*$^{-/-}$ MSCs decreased the expression of Runx2 and its target, TAZ (Fig. 2D), and other osteogenic markers such as osteocalcin (OCN), alkaline phosphatase (ALP), and collagen type I α1 (COL1A1) during osteogenic differentiation (Fig. 2E). *Pld1*$^{-/-}$ MSCs under osteogenic media for 3 days, did not affect cell proliferation, compared with that of wild type MSCs (data not shown). Similarly, PLD1 knockdown (KD) in human MSCs significantly reduced the expression of RUNX2 (Supplementary Fig. 2A), mineral deposition (Supplementary Fig. 2B), the activity of ALP (Supplementary Fig. 2C), an early marker of osteoblast differentiation, and the expression of osteogenic marker genes (Supplementary Fig. 2D). Consistently, the levels of Runx2 was greatly reduced in tibia of *Pld1*$^{-/-}$ mice as analyzed by immunofluorescence staining (Supplementary Fig. 3). Next, we investigated whether forced expression of PLD1 could rescue the promoter activity of osteogenic genes in *Pld1*$^{-/-}$ MSCs. Indeed, forced expression of PLD1 in PLD1-deficient MSCs increased the promoter activity of various osteogenic genes like Runx2, OCN, ALP, BSP, and TAZ (Fig. 2F). These results indicate that deletion of PLD1 in MSCs inhibits osteoblast differentiation.

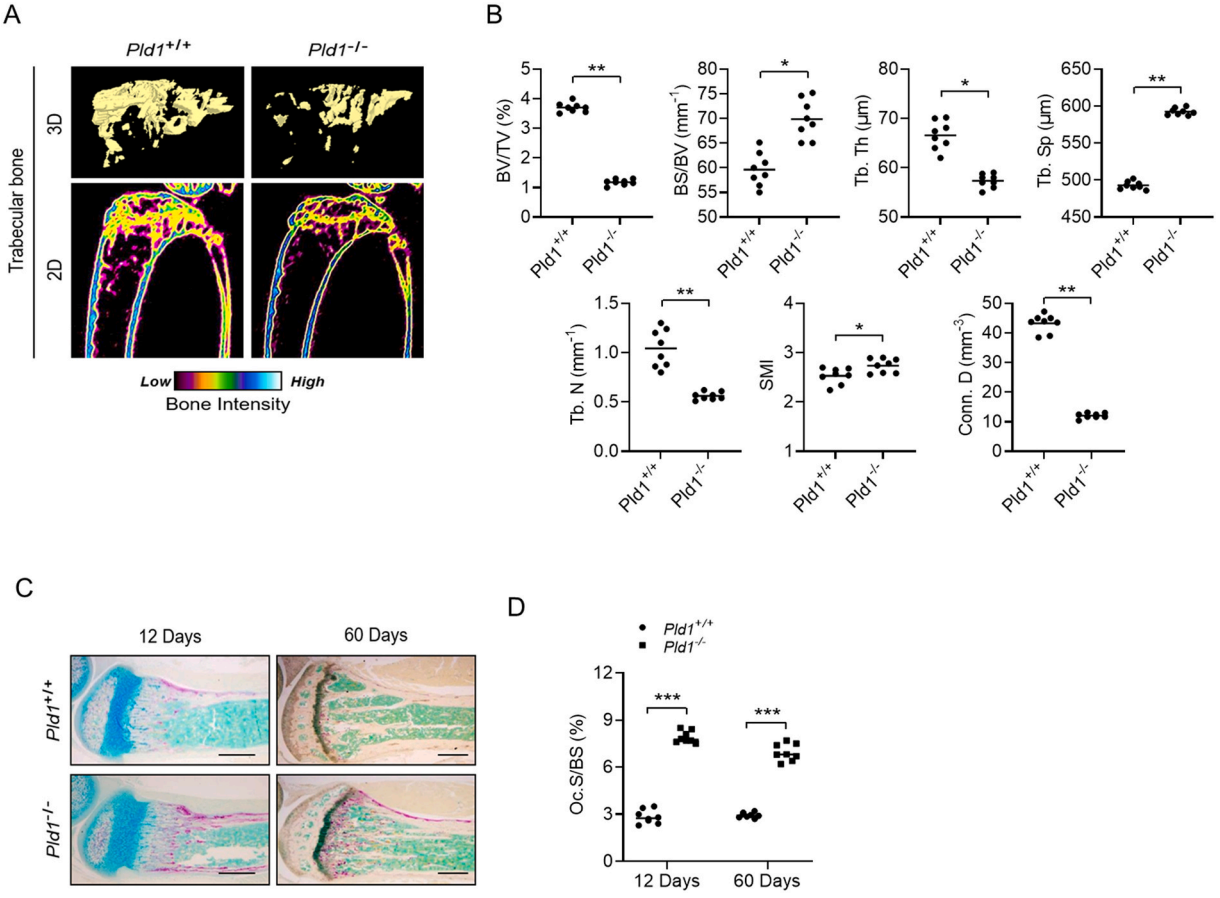

Fig. 1. Loss of PLD1 impairs bone formation.
(A) Trabecular bone structure of littermates *Pld1*$^{+/+}$ and *Pld1*$^{-/-}$ male mice, at 12 weeks of age, was analyzed by μCT and two or three-dimensional bone structure image slices were reconstructed. (B) Histomorphometric analysis of trabecular bone. $n = 8$ per group. (C) The bone structure in PLD1-deficient C57BL/6 male mice, was analyzed by TRAP staining. n = 8 per group. (D) The bone surface covered by osteoclasts was quantified. n = 8 per group. Results are representative of three independent experiments and shown as mean ± standard error of the mean (SEM). *, $P < 0.05$; **, $P < 0.01$; ***, $P < 0.001$.

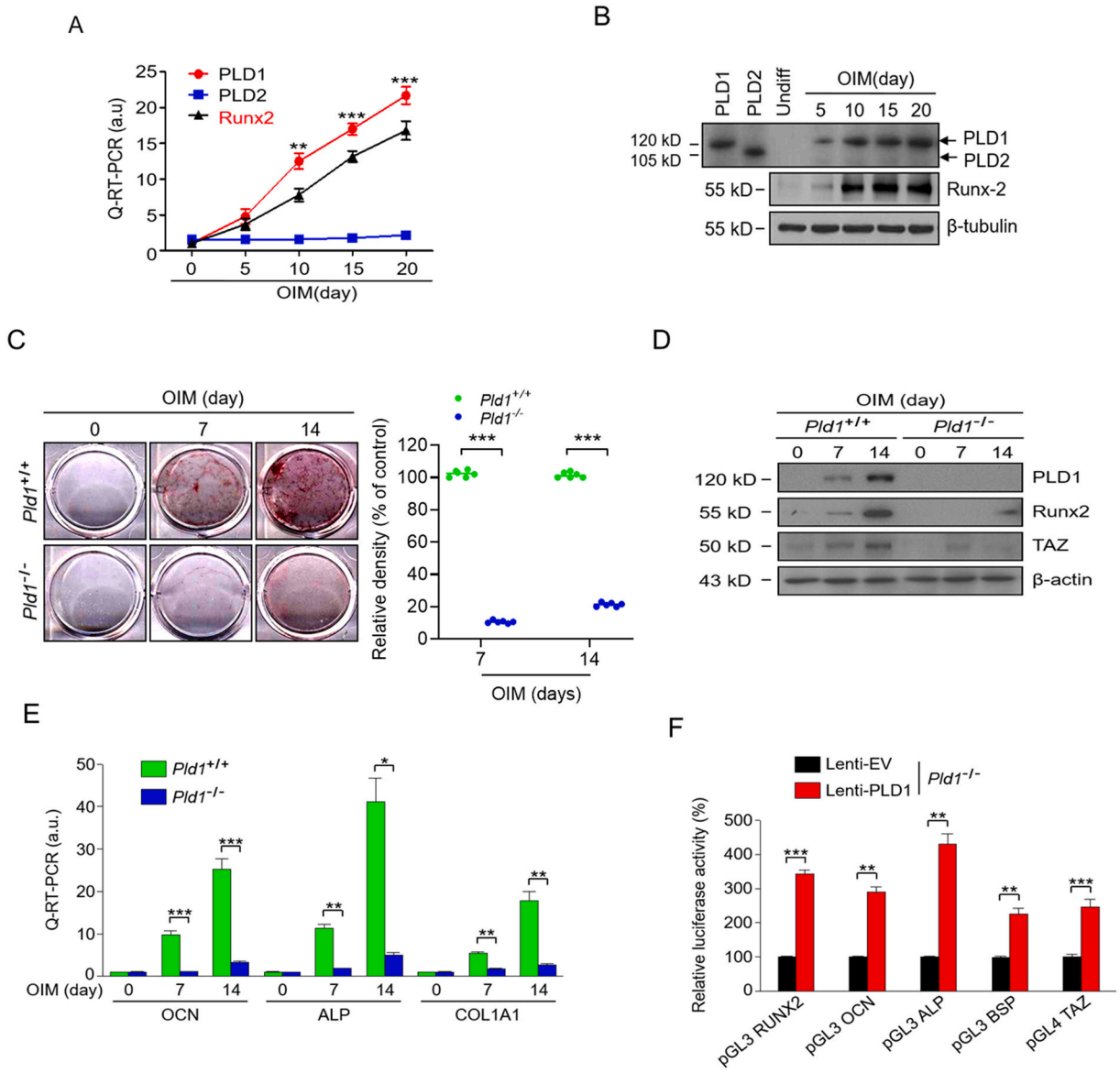

Fig. 2. Loss of PLD1 leads to decreased osteoblastogenesis.
(A,B) Osteoblast differentiation of hMSCs induced during the indicated days. Expression levels of *PLD* isozymes and *Runx2* as determined by qRT-PCR (A) and western blotting (B). (C) Osteogenic differentiation of MSCs from littermates WT and $Pld1^{-/-}$ mice as analyzed by Alizarin Red S staining (left panel) and quantification (right panel). $n = 6$ per group. (D) During osteogenesis of $Pld1^{+/+}$ and $Pld1^{-/-}$ MSCs, expression of the indicated proteins was analyzed by western blotting. (E) The expression of the indicated osteogenic marker genes during osteogenesis of mouse MSCs was analyzed by qRT-PCR. (F) Effect of PLD1 overexpression on the promoter activity of osteogenic genes in PLD1-deficient MSCs. Results are shown as mean ± SEM and are representative of at least three independent experiments. *, $P < 0.05$; **, $P < 0.01$; ***, $P < 0.001$.

3.3. PLD1 plays as a negative regulator for osteoclast differentiation and resorption activity

High TRAP (+) staining as shown in Fig. 1C suggests that low bone mass in $Pld1^{-/-}$ mice may be due to the increased osteoclast activity. Supportably, deletion of PLD1 showed a strong bone resorption activity with increased pit formation in osteoclasts derived from $Pld1^{-/-}$ bone marrow-derived macrophages (BMMs) compared to that of WT littermate mice (Fig. 3A), suggesting that PLD1 inhibits osteoclast differentiation. Since coupled bone remodeling between bone-forming osteoblasts and bone-resorbing osteoclasts is required for the maintenance of bone homeostasis [32], we performed coculture experiments using calvarial preosteoblasts (pOB) and BMMs to induce osteoclast differentiation by M-CSF and RANKL treatments. Coculture of WT pOB or BMMs with $Pld1^{-/-}$ BMMs or pOB, respectively, increased the number of TRAP-positive multinucleated osteoclasts, relative to that of coculture of *WT* pOB with *WT* BMMs (Fig. 3B). Coculture of $Pld1^{-/-}$ pOB with $Pld1^{-/-}$ BMMs showed the strongest osteoclast formation and resorption activity (Fig. 3B and C). TRAP activity showed positive correlation with osteoclast formation in the coculture of pOB and BMMs (Supplementary Fig. 4). Consistently, coculture of WT pOB or BMMs with $Pld1^{-/-}$ BMMs or $Pld1^{-/-}$ pOB, respectively, increased osteoclast resorption activity compared to that of coculture of WT pOB and WT BMMs (Fig. 3C). Moreover, these coculture experiments using WT and $Pld1^{-/-}$ pOB and BMMs showed increased expression of osteoclast differentiation markers including c-Fos, PPAR-γ, NFATc1, TRAP, Cathepsin K, and MMP-9 (Fig. 3D). Taken together, these results indicated that the increased osteoclast differentiation in $Pld1^{-/-}$ mice could be due to the contribution of both osteoblast and osteoclast lineage cells.

Next, we evaluated the role of PLD1 on estrogen deficiency-mediated

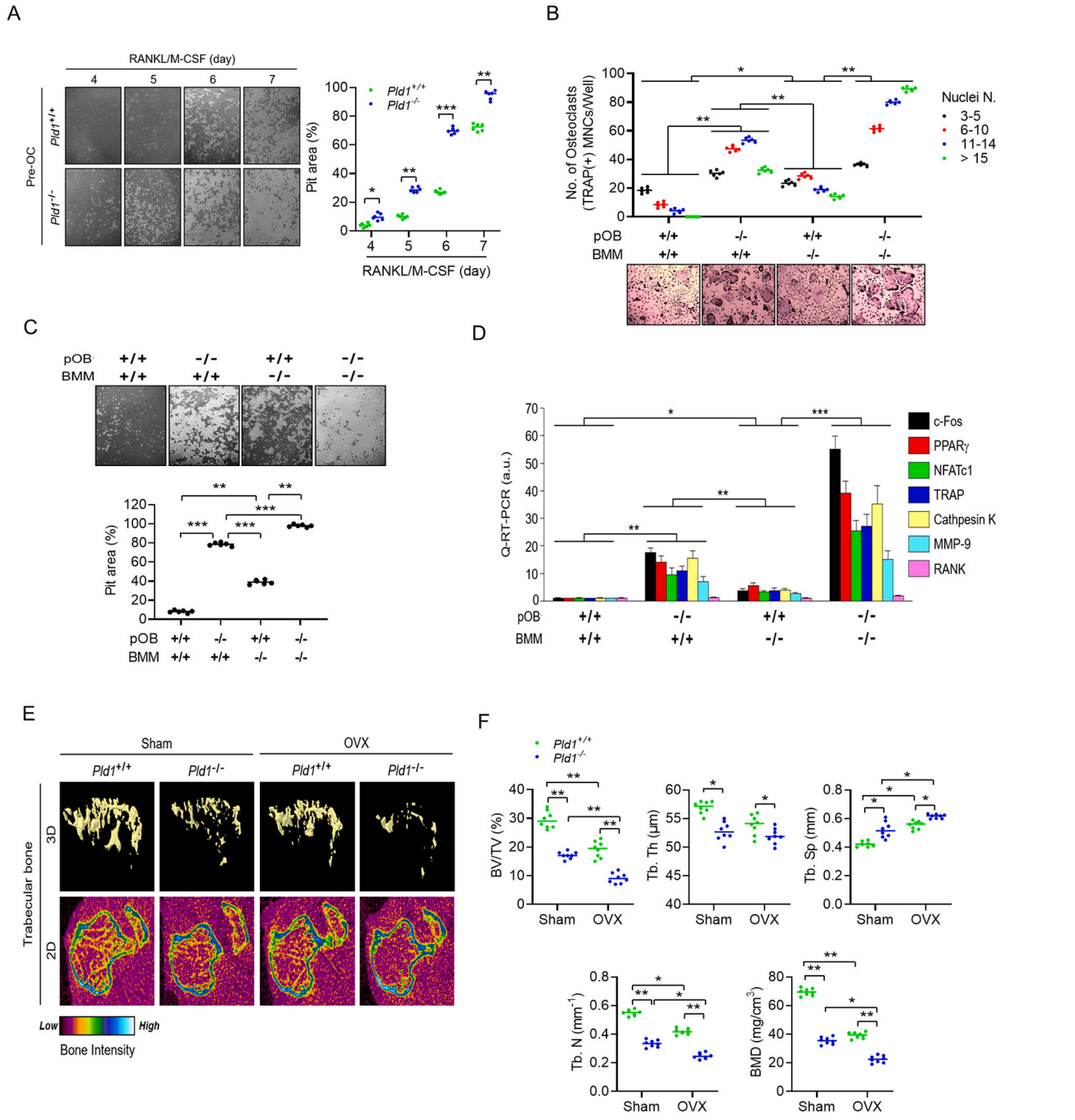

Fig. 3. Loss of PLD1 leads to increased osteoclasgogenesis.
(A) Representative images of resorption pits (left) and quantification of resorption pit area (right) during osteoclastogenesis. BMMs were cultured as shown in Materials and Methods. n = 6 per group. (B) The number of osteoclasts (upper) and representative images (lower) of BMMs in cocultures with osteoblasts originated from WT littermates (+/+) and *Pld1*$^{-/-}$ (−/−) mice. n = 6 per group. (C) Effect of coculture of WT pOB or BMMs with *Pld1*$^{-/-}$ BMMs or pOB on bone resorption. Representative images of resorption pits (left) and quantification of resorption pit area (right). n = 6 per group. (D) Expression of osteoclast differentiation markers by qRT-PCR under the indicated coculture conditions. (E) The femur bone structure of OVX female mice, at 12 weeks of age was analyzed using μCT and two or three-dimensional bone structure image slices were reconstructed (F) BMD and histomorphometric analysis of trabecular bone from OVX mice. $n = 8$ per group. Results are shown as mean ± SEM and are representative of at least three independent experiments. *, $P < 0.05$; **, $P < 0.01$; ***, $P < 0.001$.

bone loss using ovariectomized mice as a model of postmenopausal osteoporosis. Six weeks after ovariectomy (OVX), decreased femoral BV/TV, BMD, Tb.Th, Tb.N, and increased Tb.Sp in both *Pld1*$^{+/+}$ and *Pld1*$^{-/-}$ mice were observed compared to those of sham mice (Fig. 3E and F). Trabecular bone loss of *Pld1*$^{-/-}$ mice markedly increased compared with that of the control group as shown by μCT analyses (Fig. 3E and F). Taken together, these observations suggest that deletion of PLD1 accelerates osteoclast differentiation cell-autonomously and thus PLD1 is a negative regulator of osteoclast differentiation.

3.4. Reduced expression of OPG in *Pld1*$^{-/-}$ osteoblasts is associated with enhanced osteoclast differentiation

Low bone mass in *Pld1*$^{-/-}$ mice could be due to the combined

dysregulation between osteoblast and osteoclasts during bone remodeling. The observed increase in the number and bone resorption activity of osteoclasts in PLD1-deficient mice prompted us to examine the expression of osteoclastogenic and osteoblast markers, particularly with respect to the components of the RANK-RANKL signaling pathway. PLD1-deficient calvariae showed significant decrease in the expression of RANKL, OPG, and osteogenic genes, including Runx2, OCN, ALP, COL1A1, and β-catenin at the transcriptional level (Fig. 4A). PLD1-deficient calvariae also showed the protein level of β-catenin (Supplementary Fig. S5). In particular, the expression of *Opg* in *Pld1*$^{-/-}$ calvarial preosteoblasts was dramatically diminished by a factor of 30, while the expression of *Rankl* was decreased by a factor of 1.4 Hence, the RANKL/OPG ratio, an important determinant of osteoclast formation, increased approximately 18-fold in *Pld1*$^{-/-}$ calvarial osteoblasts compared to WT osteoblasts.

The increased osteoclast numbers with reduced *Opg* expression in *Pld1*$^{-/-}$ pOB, were correlated with the decreased serum OPG levels of 8-week-old *Pld1*$^{-/-}$ mice compared to that of WT mice (Fig. 4B). Moreover, treatment with OPG blocking antibody increased TRAP activity in the coculture of WT pOB and BMMs but not in the coculture of *Pld1*$^{-/-}$ osteoblasts and WT BMMs (Fig. 4C). Thus, the acceleration of osteoclast formation due to deletion of *Pld1* appears to be linked to the dramatic increase in RANKL/OPG ratio. These results further indicated that the increase in the number and activity of osteoclasts in *Pld1*$^{-/-}$ mice was due to the combined contribution of osteoblasts and osteoclasts.

3.5. *Pld1*$^{-/-}$ osteoblasts inhibits OPG expression by downregulation of β-catenin

Since β-catenin has been known to be a regulator for OPG expression [33], we examined whether β-catenin affects the promoter activity of *Opg* in *Pld1*$^{-/-}$ osteoblasts. As expected, expression of β-catenin increased the promoter activity of *Opg* (Fig. 4D). However, Runx2 did not affect *Opg* promoter activity. Mutation studies of β-catenin/TCF binding site (TBE) and Runx2 binding site (OSE) further confirmed a positive regulatory role of β-catenin in the activity of the *Opg* promoter (Fig. 4D). Deletion of PLD1 diminished OPG expression, which was recovered by overexpression of constitutive active β-catenin (Fig. 4E). Furthermore, *Pld1*$^{-/-}$ osteoblasts showed a dramatic decrease in the binding of β-catenin to the *Opg* promoter, which was recovered by forced expression of β-catenin (Fig. 4F). Taken together, these results suggest that downregulation of OPG expression in *Pld1*$^{-/-}$ osteoblasts is associated with β-catenin-pathway.

3.6. *Pld1*$^{-/-}$ osteoclast lineage cells upregulates PPAR-γ and C/EBPα mediated c-Fos expression during osteoclastogenesis

We further investigated whether the upregulation of

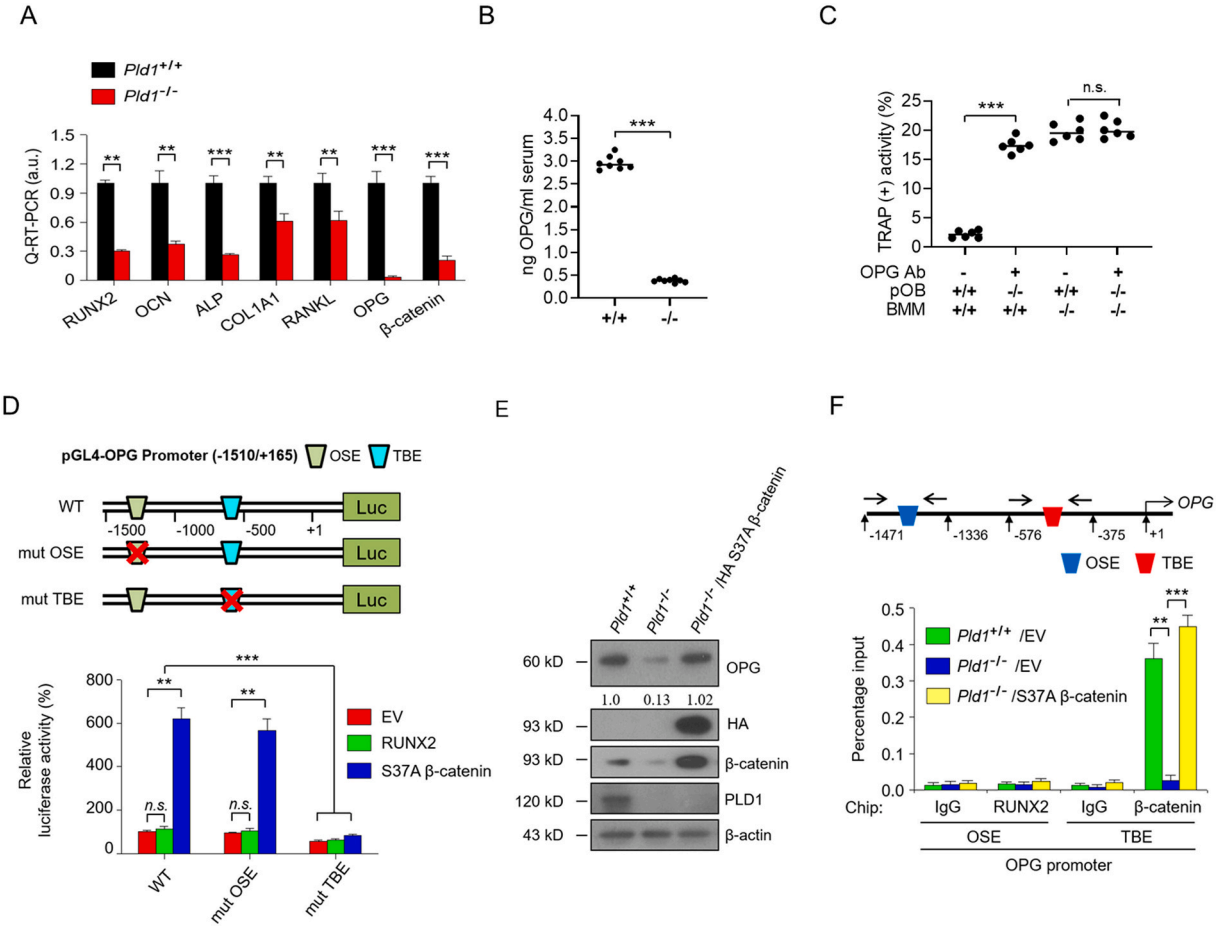

Fig. 4. Downregulation of OPG by PLD1 deficiency is mediated by β-catenin in osteoblasts.
(A) Expression of the indicated genes in neonatal calvariae from *Pld1*$^{+/+}$ and *Pld1*$^{-/-}$ mice as analyzed by qRT-PCR. (B) Determination of serum levels of OPG from WT *(+/+)* and *Pld1*$^{-/-}$ (−/−) mice by ELISA. n = 8 per group. (C) TRAP activity assay of BMMs in coculture with osteoblasts in the presence of OPG blocking antibody. n = 6 per group. (D) Schematic representation of putative Runx2-binding element (OSE) and TCF-binding element (TBE) in the *Opg* promoter region (top). Effect of Runx2 and β-catenin on the promoter activity of OPG (bottom). (E) Effect of β-catenin overexpression on the protein level of OPG in *Pld1*$^{-/-}$ osteoblasts. (F) ChIP assay for the binding of β-catenin to the promoter of *Opg* in *Pld1*$^{-/-}$ osteoblasts. Results are shown as mean ± SEM and are representative of at least three independent experiments. *, $P < 0.05$; **, $P < 0.01$; ***, $P < 0.001$.

osteoclastogenesis in *Pld1*$^{-/-}$ BMMs was due to the deregulation of osteoclast lineage cells. *Pld1*$^{-/-}$ calvariae showed significant increase in osteoclastogenic markers including c-Fos, NFATc1, TRAP, and Cathepsin K, suggesting a negative role of PLD1 on osteoclastogenesis (Fig. 5A). Moreover, during osteoclastic differentiation of RANKL/M-CSF-treated BMMs, expression of β-catenin and RUNX2 did not affect expression of osteoclastogenic markers increased in PLD1-deficient BMMs (Supplementary Fig. 6A), suggesting involvement of other factor (s) in the regulation of osteoclastogenesis by PLD1. As a control, expression of β-catenin and RUNX2 is shown in Supplementary Fig. 6b. Interestingly, loss of PLD1 increased expression of PPAR-γ and C/EBPα in calvariae (Fig. 5A). PPAR-γ and C/EBPα, well-known master regulators of adipogenesis, have been known as upregulator for c-Fos expression, an essential mediator of osteoclastogenesis [5–7]. Therefore, we further investigated whether PPAR-γ and C/EBPα could affect *c-fos* promoter activity in BMMs. Based on the bioinformatic analysis we found that there were two binding sites of PPAR-γ and C/EBPα on the *c-fos* promoter. As analyzed by chromatin immunoprecipitation (ChIP) assay, PLD1 ablation enhanced the binding of PPAR-γ and C/EBPα to the *c-fos* promoter, which was suppressed by shRNAs for PPAR-γ and C/EBPα Fig. 5B). In RANKL/M-CSF-treated BMMs, PLD1 deletion significantly increased the expression of PPAR-γ and C/EBPα Fig. 5C as well as promoter activity of *c-fos*, which was reduced by depletion of PPAR-γ and C/EBPα (Fig. 5D). Taken together, these results indicate that PLD1-deficient osteoclast lineage cells promote osteoclast differentiation via upregulation of PPAR-γ and C/EBPα-induced c-Fos expression.

3.7. Increased fat mass and adipogenesis in *Pld1*$^{-/-}$ mice

As shown in Fig. 5, deficiency of PLD1 increased the expression of PPAR-γ and C/EBPα in calvarial bone. Thus, we hypothesized that PLD1 might also play a role as a regulatory switch between osteoblastogenesis and adipogenesis. Although body weight of *Pld1*$^{-/-}$ mice did not differ from that of WT littermate mice until 180 days of age, it was slightly increased in *Pld1*$^{-/-}$ mice at 200 days of age (Fig. 6A). Interestingly, the loss of PLD1 increased the weight of white adipose tissues (WAT) and brown adipose tissues (BAT) over time in a linear and U-shaped pattern, respectively (Fig. 6B). We further confirmed the increase in lipid droplet size in eWAT and BAT from *Pld1*$^{-/-}$ mice, relative to *Pld1*$^{+/+}$ mice, as analyzed by Oil Red O staining (Fig. 6C). Besides, the number of average white and brown adipocytes in *Pld1*$^{-/-}$ mice was increased compared to that of *Pld1*$^{+/+}$ mice (Supplementary Fig. 7). Tomography images indicated that *Pld1*$^{-/-}$ mice at the age of 45, 90, and 150 days showed significant increase in abdominal fat volume (Fig. 6D). We further investigated the expression of PLD1 during adipogenic differentiation of MSCs. The expression of PLD1 was gradually increased during adipogenesis of MSCs (Supplementary Fig. 9). As a control, the expression of C/EBPα was increased during adipogenesis. Furthermore, PLD1 ablation increased the expression of major adipogenic or lipogenic transcription factors such as PPAR-γ, C/EBPα and sterol regulatory element binding protein 1c (SREBP1c) in BAT, WAT, and even liver, as analyzed by qRT-PCR (Fig. 6E) and immunofluorescence staining (Supplementary Fig. 8A and 8B). The Wnt/β-catenin signaling pathway has been known to repress adipogenesis by blocking the induction of PPAR-γ and C/EBPα [34]. Loss of PLD1 decreased the expression of β-catenin in eWAT, BAT and liver (Fig. 6E, Supplementary Fig. 8B). Recently, we reported that

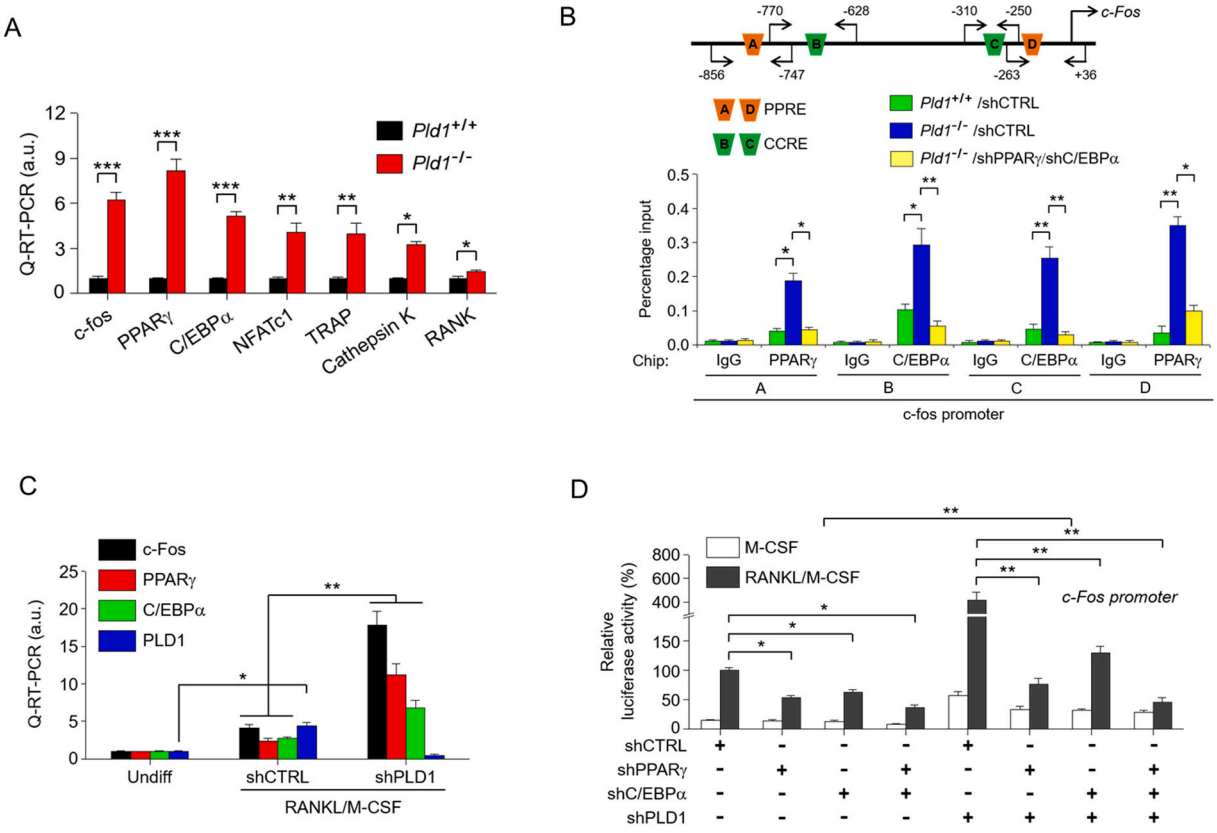

Fig. 5. PLD1 ablation in osteoclast lineage cells upregulates PPAR-γ and C/EBPα mediated c-Fos expression during osteoclastogenesis.
(A) qRT-PCR of osteoclastogenic markers in neonatal calvariae from *Pld1*$^{+/+}$ littermates and *Pld1*$^{-/-}$ mice. (B) *Pld1*$^{-/-}$ BMMs were infected with lentiviral vector expressing control (CTRL), *Ppar-γ* or *Cebpα* knockdown (KD) shRNAs, followed by ChIP assay for the binding of PPAR-γ and C/EBPα to the promoter of *c-fos*. (C) Effect of PLD1 deletion on the expression of *c-fos, Ppar-γ, Cebpα* in RANKL/M-CSF-treated BMMs. (D) Effect of inhibition of *c-fos, Ppar-γ, Cebpα* genes on the promoter activity of c-Fos. Results are shown as mean ± SEM and are representative of at least three independent experiments. *, $P < 0.05$; **, $P < 0.01$; ***, $P < 0.001$.

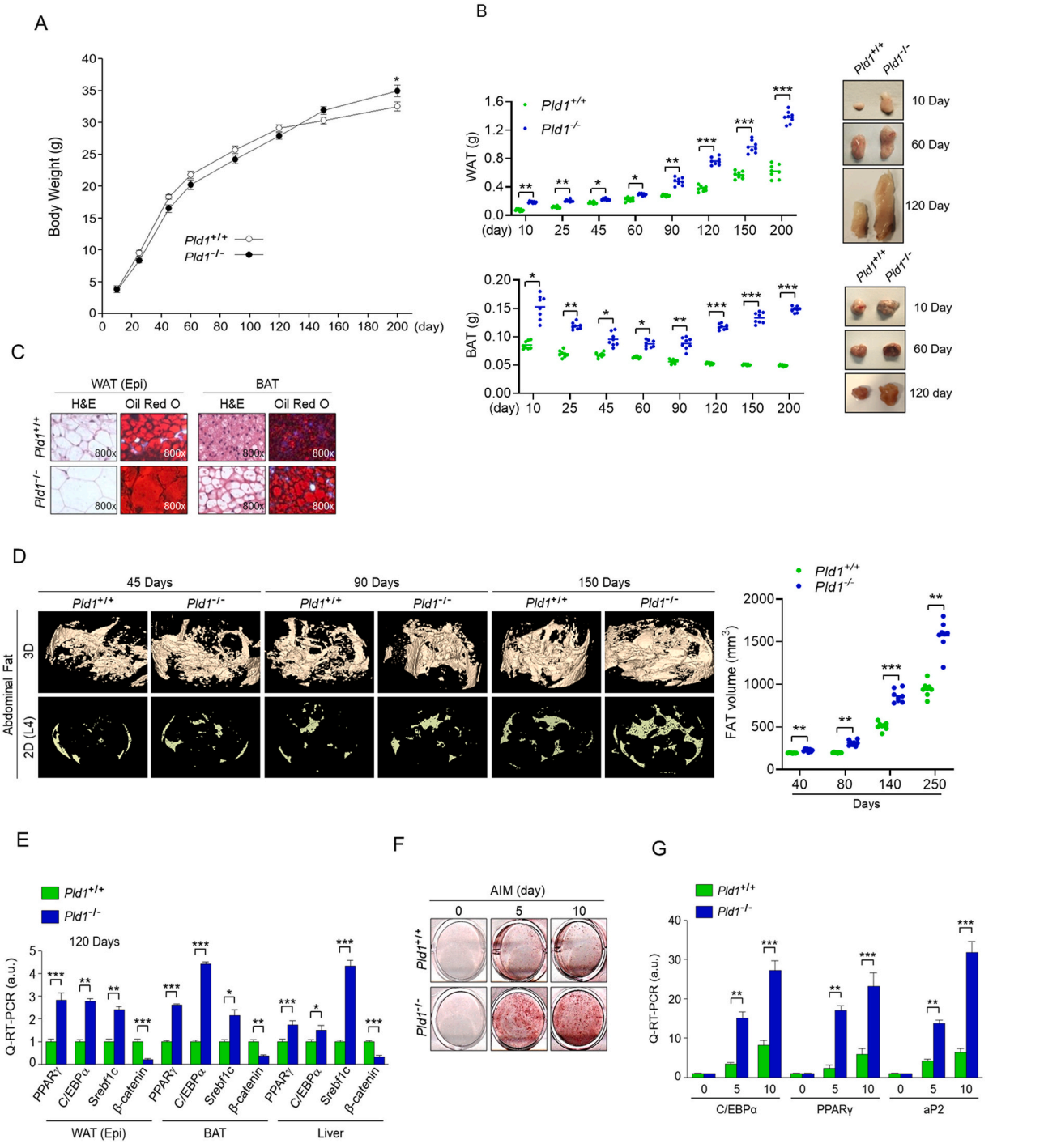

Fig. 6. Ablation of PLD1 increases fat mass and adipogenesis.
(A) Total body weight of *Pld1*$^{+/+}$ and *Pld1*$^{-/-}$ mice. (B) The weight and representative images of WAT (upper) and BAT (lower) from the indicated age of male mice. n = 8 per group. (C) Representative images of hematoxylin and eosin (H&E) and Oil Red O staining in WAT and BAT. (D) Micro-CT analysis of abdominal fat structure and reconstruction of two or three-dimensional fat structure image slices of the indicated age of male mice (left), and quantification of fat volume (right). n = 8 per group. (E) qRT-PCR of *Ppar-γ*, *Cebpα*, *Srebp1c*, and *Ctnnb1* expression in WAT, BAT, and liver. *Pld1*$^{-/-}$ MSCs were differentiated into adipocytes for the indicated time and analyzed by Oil Red O staining (F) and qRT-PCR of adipogenesis marker genes (G). Results are shown as mean ± SEM and are representative of at least three independent experiments. *, $P < 0.05$; **, $P < 0.01$; ***, $P < 0.001$.

pharmacological inhibition of PLD1 reduces the expression of β-catenin at the post-transcriptional level in cancer cells [35]. In addition to adipocytes, PLD1 ablation significantly increased the expression of adipogenic genes including PPAR-γ, C/EBPα, and aP2 in MSCs compared to that of WT mice (Fig. 6F and G). To further clarify the effect of β-catenin on adipogenesis of PLD1 KO MDCs, we examined whether overexpression of β-catenin downregulates the expression of C/EBPα and PPARγ Forced expression of β-catenin in PLD1 KO MSCs reduced the protein levels of C/EBPα and PPARγ (Supplementary Fig. 10). Taken together, these data suggest that PLD1 ablation increases fat mass and adipogenesis via upregulation of major adipogenic transcription factors in both MSCs and adipose tissues.

3.8. Adipocyte-specific PLD1 overexpression decreases fat mass and adipogenesis in *Pld1*$^{-/-}$ mice

To further study the role of PLD1 in adipose tissues, we generated PLD1-Ap2 transgenic (*Pld1*^{Tg}) mice that overexpress GFP-PLD1 specifically in adipocytes. The transgenic mice exhibited high GFP-PLD1 expression in adipose tissues but not in other organs (Fig. 7A). To explore the impact of adipocyte-specific PLD1 overexpression in *Pld1*$^{-/-}$ mice, *Pld1*$^{-/-}$*Pld1*^{Tg} mice were generated by crossing *Pld1*^{Tg} with *Pld1*$^{-/-}$ mice. *Pld1*$^{-/-}$*Pld1*^{Tg} mice significantly decreased the mass of WAT and BAT at all the examined ages, compared to those of *Pld1* $^{-/-}$ mice (Fig. 7B). Moreover, analysis of WAT and BAT sections from *Pld1*$^{-/-}$*Pld1*^{Tg} mice, taken 160 days after birth, showed decrease in lipid droplet size, relative to *Pld1*$^{-/-}$ mice (Fig. 7C). In addition, the number of average white and brown adipocytes in *Pld1*$^{-/-}$*Pld1*^{Tg} mice was decreased compared to that of *Pld1*$^{-/-}$ mice (Supplementary Fig. 11). Abdominal fat depots were significantly decreased in *Pld1*$^{-/-}$*Pld1*^{Tg} mice compared to that of *Pld1* $^{-/-}$ mice at 90 and 160 days after birth, as analyzed by μCT (Fig. 7D). Furthermore, adipocyte-specific PLD1 overexpression in *Pld1*$^{-/-}$ mice reduced the expression of PPAR-γ, C/EBPα, and SREBP1 in WAT, BAT and liver, but increased the level of β-catenin, compared to that of *Pld1*$^{-/-}$ mice (Fig. 7E). Interestingly, *Pld1*$^{-/-}$*Pld1*^{Tg} mice at 160 days greatly suppressed the phenotype of hepatic steatosis observed upon PLD1 ablation (Supplementary Fig. 12A). The activities of alanine aminotransferase (ALT) and aspartate aminotransferase (AST), two of the most reliable markers of hepatocellular injury, were increased in the serum of *Pld1*$^{-/-}$ mice, suggesting liver dysfunction in these mice (Supplementary Fig. 12B). However, adipocyte-specific PLD1 overexpression in *Pld1*$^{-/-}$ mice reduced the levels of hepatic triacylglycerol, cholesterol, and the activities of ALT and AST, relative to *Pld1*$^{-/-}$ mice (Supplementary Fig. 12B). Taken together, these results indicate that adipocyte-specific PLD1 overexpression decreases fat mass and adipogenesis in *Pld1*$^{-/-}$ mice.

4. Discussion

In this study, we demonstrate that deletion of PLD1 stimulates the conversion of MSCs into more adipogenic pathway than osteogenic one,

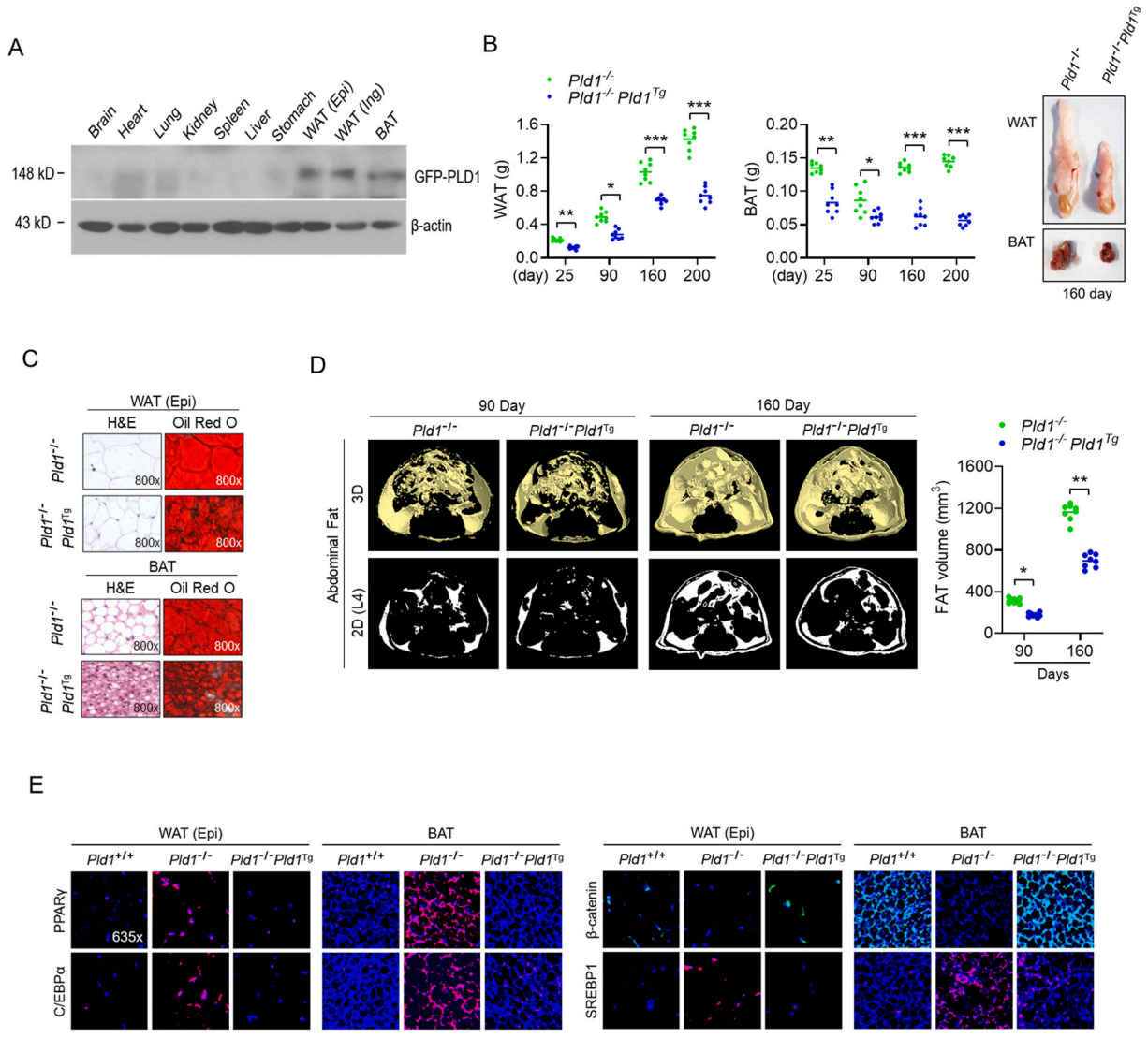

Fig. 7. Adipocyte-specific PLD1 overexpression decreases fat mass and adipogenesis in *Pld1*$^{-/-}$ mice.
(A) Expression of PLD1 in various tissues from *Pld1*^{Tg} mice. (B) The mass of WAT and BAT from *Pld1*$^{-/-}$ and *Pld1*$^{-/-}$*Pld1*^{Tg} male mice at the indicated ages. n = 8 per group (C) Representative images of H&E and Oil Red O staining in WAT and BAT of the indicated male mice. (D) Analysis of abdominal fat depots by two or three-dimensional μCT from male mice at the indicated ages and quantification of fat volume. n = 8 per group (E) Immunofluorescent staining to detect the expression of PPAR-γ and C/EBPα in WAT and BAT. Results are shown as mean ± SEM and are representative of at least three independent experiments. *, $P < 0.05$; **, $P < 0.01$; ***, $P < 0.001$.

which resulted in the diminished bone mass but increased fat mass.

It was suggested that PLD might be involved in bone formation, as evidenced by its expression and activity in osteoblasts and osteoclasts [19–22]. In addition, it was reported that PLD regulated adiopogenic differentiation in cultured cells [36]. However, the functional roles of PLD in bone remodeling and adipogenic function in vivo animal model, remain unknown. Thus, we tried to investigate the role of PLD1 in bone and fat homeostasis using PLD1 KO mice. *Pld1*$^{-/-}$ mice had reduced bone mass due to increased number and activity of osteoclasts as well as diminished osteoblast differentiation. Upregulation of osteoclastogenic activity by PLD1 deficiency was due to both the increased RANKL/OPG ratio through the reduced expression of β-catenin in osteoblast lineage cells and enhanced expression of PPAR-γ and C/EBPα mediated c-Fos in osteoclast lineage cells. Moreover, loss of PLD1 increased adipogenesis, body fat mass, and hepatic steatosis along with upregulation of PPAR-γ and C/EBPα. The reduced expression of PLD is involved in the replicative and premature senescence in human fibroblasts [37]. Recently, it has been reported that PLD1 but not PLD2 enhances the mineralization in osteoblasts [22]. Although PLD1 inhibitor-treated and PLD1-deficient osteoblasts were significantly less efficient in mineralization, bone formation was not impaired in PLD1 KO mice [24]. They performed the experiments using small number of female mice ($n = 4$) at 6–12 months without examination of the effects of PLD1 on osteoclast differentiation [22]. Thus, the finding should be interpreted with caution. With regard to bone mass, our *Pld1*$^{-/-}$ C57BL/6 mice showed low bone mass clearly compared to WT littermate mice. At present, we do not figure out why these two results are different. It may be due to differences in the gender, strains, age, and housing condition of mice. The coordinated action of osteoblasts and osteoclasts controls bone architecture. Female and male have very different bone homeostasis, and age can affect bone homeostasis too. In our study we utilized male mice and OVX female mice ($n = 8$) at 8–12 weeks and investigated the effect of PLD1 ablation on the activity of both osteoblasts and osteoclasts. Based on our results, low bone mass owing to ablation of PLD1 was due to the defects in both osteoblasts and osteoclasts, implicating the importance of coupling between osteoblasts and osteoclasts during bone remodeling [32]. An accelerated bone loss even under estrogen deficiency in *Pld1*$^{-/-}$ mice was due to the several reasons. First, the RANKL/OPG ratio was increased in *Pld1*$^{-/-}$ mice. Since OPG suppresses the RANK-RANKL signaling pathway [13,38], a dramatic decrease in OPG levels by downregulation of β-catenin in *Pld1*$^{-/-}$ preosteoblasts was responsible for acceleration of osteoclast activity. Interestingly, human MSCs gradually decreased expression of osteogenic markers as well as OPG with aging [39]. Our previous study showed that PLD1 inhibition increased expression of miRNA-4496 that causes downregulation of β-catenin in cancer cells [35]. With respect to the PLD1-mediated regulation of β-catenin expression via miRNAs, further studies are required in osteoblasts. Secondly, ablation of PLD1 also promoted osteoclastogenesis cell-autonomously via upregulation of PPAR-γ and C/EBPα-induced c-fos in osteoclast lineage cells. Using PLD1 knockout mice, we showed that PLD1 controlled differentiation of MSCs into osteoblasts and adipocytes via downregulation of osteogenic (RUNX2) and upregulation of adipogenic (PPAR-γ, C/EBPα) transcription factors (Fig. 8). Although the molecular mechanisms of PLD1-mediated *Runx2* expression have not been determined, reduction of Runx2 and its target genes by deletion of PLD1 may provide an explanation for suppression of osteoblast differentiation. PLD1 was upregulated during osteoblastogenesis. Elucidation of the mechanisms by which PLD1 affects Runx2 expression requires further studies. An inverse relationship between adipogenesis and osteogenesis leads to the concept that inhibition of adipogenesis might enhance bone formation [40]. In this study, ablation of PLD1 increased adipogenesis of MSCs, fat mass, adipocyte size, and lipid droplets in WAT, BAT, and liver. Moreover, overexpression of PLD1 in adipocyte of PLD1 null mice rescued fat mass observed in *Pld1*$^{-/-}$ mice. Thus, it is suggested that PLD1 plays a positive and negative role on bone and fat tissues, respectively (Fig. 8). Deletion of PLD1 upregulated expression of

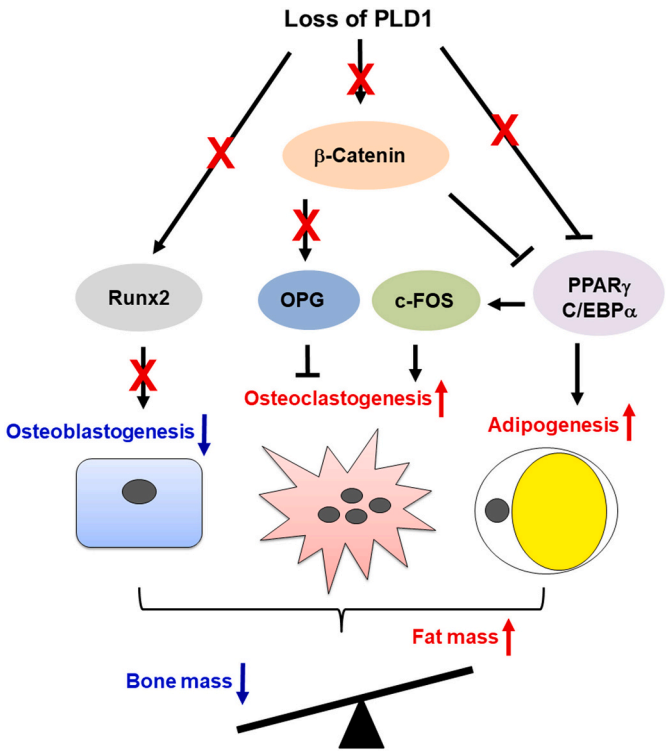

Fig. 8. Schematic diagram representing the proposed mechanisms for PLD1-mediated bone and adipose tissue homeostasis.
PLD1 induces osteogenesis via upregulation of Runx2 and suppresses osteoclastogenesis via upregulation of β-catenin-mediated OPG expression and downregulation of PPAR-γ and C/EBPα-induced c-Fos. Furthermore, PLD1 suppresses adipogenesis via upregulation of PPAR-γ and C/EBPα. PLD1 deficiency disrupts the balance between bone and fat mass, resulting in low bone mass and high fat mass. PLD1 may be a novel regulator of bone and fat homeostasis.

PPAR-γ, C/EBPα, and SREBP1, but downregulated β-catenin expression. Although the Wnt-β-catenin signaling pathway is known to suppress adipogenesis by reducing the expression of PPAR-γ and C/EBPα [41], the mechanism of this suppression remains to be elucidated at the molecular level. The decrease in bone mass and increase in fat mass in *Pld1*$^{-/-}$ mice are similar to changes associated with osteoporosis and age-related osteopenia [42]. Unbalanced differentiation of MSCs into adipocytes rather than osteoblasts might be a causing factor for osteoporosis and aging [3]. Osteoporotic bones contain aberrantly high numbers of adipocytes in the trabecular bone marrow space [43] and increased bone marrow fat is a consequence or the cause of decreased bone mass in osteoporosis [44]. Interestingly, bone marrow fat-secreted factors could be biomarkers for detection of bone marrow adipose tissue accumulation and osteoporosis risk [45]. The phenotype of hepatic steatosis in *Pld1*$^{-/-}$ mice might be due to secretory factor(s) released from various adipose tissues including bone marrow fat. Non-alcoholic fatty liver disease is associated with hepatic insulin resistance, which is a major risk factor for type 2 diabetes [46]. Therefore, tissue-specific conditional PLD1 knockout is necessary for further identification of a new role of PLD1 in bone diseases as well as other metabolic diseases. Collectively, these results indicate that PLD1 plays a positive and negative role in maintaining bone and fat mass by regulating osteoblasts and adipocytes, respectively.

5. Conclusions

This study identifies PLD1 as a key novel regulator of bone homeostasis and adipogenic function through Runx2, β-catenin-OPG, PPAR-γ

and C/EBPα axis. PLD1 regulated the bifurcating pathways of mesenchymal stem cell lineage into increased osteogenesis and decreased adipogenesis, which uncovered a hitherto unrecognized role of PLD1 in homeostasis between bone and fat mass.

CRediT authorship contribution statement

Dong Woo Kang: Conceptualization, Investigation. **Won Chan Hwang:** Investigation. **Yu Na Noh:** Investigation. **Xiangguo Che:** Investigation. **Soung-Hoon Lee:** Investigation. **Younghoon Jang:** Investigation. **Kang-Yell Choi:** Formal analysis, Writing-review and editing. **Je-Yong Choi:** Formal analysis, Writing-review and editing. **Do Sik Min:** Conceptualization, Funding acquisition, Formal analysis, Writing-original draft, Writing-review and editing, Supervision.

Declaration of competing interest

The authors declare that they have no known competing financial interests or personal relationships that could have appeared to influence the work reported in this paper.

Acknowledgments

This work was supported by the National Research Foundation of Korea (NRF) grant funded by the Korean government (NRF-2018R1A2B3002179) and by the Yonsei University Research Fund of 2019-22-0193.

Appendix A. Supplementary data

Supplementary data to this article can be found online at https://doi.org/10.1016/j.bbadis.2021.166084.

References

[1] A. Uccelli, L. Moretta, V. Pistoia, Mesenchymal stem cells in health and disease, Nat. Rev. Immunol. 8 (2008) 726–736.
[2] P. Meunier, J. Aaron, C. Edouard, G. Vignon, Osteoporosis and the replacement of cell populations of the marrow by adipose tissue. A quantitative study of 84 iliac bone biopsies, Clin. Orthop. Relat. Res. 80 (1971) 147–154.
[3] J.M. Gimble, S. Zvonic, Z.E. Floyd, M. Kassem, M.E. Nuttall, Playing with bone and fat, J. Cell. Biochem. 98 (2006) 251–266.
[4] E.D. Rosen, O.A. MacDougald, Adipocyte differentiation from the inside out, Nat. Rev. Mol. Cell Biol. 7 (2006) 885–896.
[5] Y. Wan, L.W. Chong, R.M. Evans, PPAR-gamma regulates osteoclastogenesis in mice, Nat. Med. 13 (2007) 1496–1503.
[6] W. Chen, G. Zhu, L. Hao, M. Wu, H. Ci, Y.P. Li, C/EBPalpha regulates osteoclast lineage commitment, Proc. Natl. Acad. Sci. U. S. A. 110 (2013) 7294–7299.
[7] A.E. Grigoriadis, Z.Q. Wang, M.G. Cecchini, W. Hofstetter, R. Felix, H.A. Fleisch, E. F. Wagner, C-Fos: a key regulator of osteoclast-macrophage lineage determination and bone remodeling, Science (New York, N.Y.) 266 (1994) 443–448.
[8] T. Akune, S. Ohba, S. Kamekura, M. Yamaguchi, U.I. Chung, N. Kubota, Y. Terauchi, Y. Harada, Y. Azuma, K. Nakamura, T. Kadowaki, H. Kawaguchi, PPARgamma insufficiency enhances osteogenesis through osteoblast formation from bone marrow progenitors, J. Clin. Invest. 113 (2004) 846–855.
[9] S. Kang, C.N. Bennett, I. Gerin, L.A. Rapp, K.D. Hankenson, O.A. Macdougald, Wnt signaling stimulates osteoblastogenesis of mesenchymal precursors by suppressing CCAAT/enhancer-binding protein alpha and peroxisome proliferator-activated receptor gamma, J. Biol. Chem. 282 (2007) 14515–14524.
[10] F. Otto, A.P. Thornell, T. Crompton, A. Denzel, K.C. Gilmour, I.R. Rosewell, G. W. Stamp, R.S. Beddington, S. Mundlos, B.R. Olsen, P.B. Selby, M.J. Owen, Cbfa1, a candidate gene for cleidocranial dysplasia syndrome, is essential for osteoblast differentiation and bone development, Cell 89 (1997) 765–771.
[11] T. Komori, H. Yagi, S. Nomura, A. Yamaguchi, K. Sasaki, K. Deguchi, Y. Shimizu, R. T. Bronson, Y.H. Gao, M. Inada, M. Sato, R. Okamoto, Y. Kitamura, S. Yoshiki, T. Kishimoto, Targeted disruption of Cbfa1 results in a complete lack of bone formation owing to maturational arrest of osteoblasts, Cell 89 (1997) 755–764.
[12] J.Y. Choi, J. Pratap, A. Javed, S.K. Zaidi, L. Xing, E. Balint, S. Dalamangas, B. Boyce, A.J. van Wijnen, J.B. Lian, J.L. Stein, S.N. Jones, G.S. Stein, Subnuclear targeting of Runx/Cbfa/AML factors is essential for tissue-specific differentiation during embryonic development, Proc. Natl. Acad. Sci. U. S. A. 98 (2001) 8650–8655.
[13] M.J. Jeon, J.A. Kim, S.H. Kwon, S.W. Kim, K.S. Park, S.W. Park, S.Y. Kim, C.S. Shin, Activation of peroxisome proliferator-activated receptor-gamma inhibits the Runx2-mediated transcription of osteocalcin in osteoblasts, J. Biol. Chem. 278 (2003) 23270–23277.
[14] T.L. Burgess, Y. Qian, S. Kaufman, B.D. Ring, G. Van, C. Capparelli, M. Kelley, H. Hsu, W.J. Boyle, C.R. Dunstan, S. Hu, D.L. Lacey, The ligand for osteoprotegerin (OPGL) directly activates mature osteoclasts, J. Cell Biol. 145 (1999) 527–538.
[15] W.J. Boyle, W.S. Simonet, D.L. Lacey, Osteoclast differentiation and activation, Nature 423 (2003) 337–342.
[16] R.K. Nelson, M.A. Frohman, Physiological and pathophysiological roles for phospholipase D, J. Lipid Res. 56 (2015) 2229–2237.
[17] D.W. Kang, K.Y. Choi, S. Min Do, Functional regulation of phospholipase D expression in cancer and inflammation, J. Biol. Chem. 289 (2014) 22575–22582.
[18] H.A. Brown, P.G. Thomas, C.W. Lindsley, Targeting phospholipase D in cancer, infection and neurodegenerative disorders, Nat. Rev. Drug Discov. 16 (2017) 351–367.
[19] Y.L. Hsu, J.Y. Hung, Y.C. Ko, C.H. Hung, M.S. Huang, P.L. Kuo, Phospholipase D signaling pathway is involved in lung cancer-derived IL-8 increased osteoclastogenesis, Carcinogenesis 31 (2010) 587–596.
[20] M.K. Park, Y.M. Her, M.L. Cho, H.J. Oh, E.M. Park, S.K. Kwok, J.H. Ju, K.S. Park, D. S. Min, H.Y. Kim, S.H. Park, IL-15 promotes osteoclastogenesis via the PLD pathway in rheumatoid arthritis, Immunol. Lett. 139 (2011) 42–51.
[21] M.K. Shin, Y.H. Jang, H.J. Yoo, D.W. Kang, M.H. Park, M.K. Kim, J.H. Song, S. D. Kim, G. Min, H.K. You, K.Y. Choi, Y.S. Bae, S. Min do, N-formyl-methionyl-leucyl-phenylalanine (fMLP) promotes osteoblast differentiation via the N-formyl peptide receptor 1-mediated signaling pathway in human mesenchymal stem cells from bone marrow, J. Biol. Chem. 286 (2011) 17133–17143.
[22] D. Abdallah, N. Skafi, E. Hamade, M. Borel, S. Reibel, N. Vitale, A. El Jamal, C. Bougault, N. Laroche, L. Vico, B. Badran, N. Hussein, D. Magne, R. Buchet, L. Brizuela, S. Mebarek, Effects of phospholipase D during cultured osteoblast mineralization and bone formation, J. Cell. Biochem. 120 (2019) 5923–5935.
[23] D.S. Min, B.H. Ahn, D.J. Rhie, S.H. Yoon, S.J. Hahn, M.S. Kim, Y.H. Jo, Expression and regulation of phospholipase D during neuronal differentiation of PC12 cells, Neuropharmacology 41 (2001) 384–391.
[24] C. Dall'Armi, A. Hurtado-Lorenzo, H. Tian, E. Morel, A. Nezu, R.B. Chan, W.H. Yu, K.S. Robinson, O. Yeku, S.A. Small, K. Duff, M.A. Frohman, M.R. Wenk, A. Yamamoto, G. Di Paolo, The phospholipase D1 pathway modulates macroautophagy, Nat. Commun. 1 (2010) 142.
[25] M.L. Bouxsein, S.K. Boyd, B.A. Christiansen, R.E. Guldberg, K.J. Jepsen, R. Müller, Guidelines for assessment of bone microstructure in rodents using micro-computed tomography, Journal of bone and mineral research : the official journal of the American Society for Bone and Mineral Research 25 (2010) 1468–1486.
[26] N.R. Park, K.E. Lim, M.S. Han, X. Che, C.Y. Park, J.E. Kim, I. Taniuchi, S.C. Bae, J. Y. Choi, Core binding factor beta plays a critical role during chondrocyte differentiation, J. Cell. Physiol. 231 (2016) 162–171.
[27] M. Takami, J.T. Woo, N. Takahashi, T. Suda, K. Nagai, Ca2+-ATPase inhibitors and Ca2+−ionophore induce osteoclast-like cell formation in the cocultures of mouse bone marrow cells and calvarial cells, Biochem. Biophys. Res. Commun. 237 (1997) 111–115.
[28] X.D. Chen, L.W. Fisher, P.G. Robey, M.F. Young, The small leucine-rich proteoglycan biglycan modulates BMP-4-induced osteoblast differentiation, FASEB journal : official publication of the Federation of American Societies for Experimental Biology 18 (2004) 948–958.
[29] T.L. McCarthy, M. Centrella, E. Canalis, Further biochemical and molecular characterization of primary rat parietal bone cell cultures, Journal of bone and mineral research : the official journal of the American Society for Bone and Mineral Research 3 (1988) 401–408.
[30] A. Aldridge, D. Kouroupis, S. Churchman, A. English, E. Ingham, E. Jones, Assay validation for the assessment of adipogenesis of multipotential stromal cells—a direct comparison of four different methods, Cytotherapy 15 (2013) 89–101.
[31] A. Bernhardt, K. Koperski, M. Schumacher, M. Gelinsky, Relevance of osteoclast-specific enzyme activities in cell-based in vitro resorption assays, European cells & materials 33 (2017) 28–42.
[32] N.A. Sims, T.J. Martin, Osteoclasts provide coupling signals to osteoblast lineage cells through multiple mechanisms, Annu. Rev. Physiol. 82 (2020) 507–529.
[33] D.A. Glass 2nd, P. Bialek, J.D. Ahn, M. Starbuck, M.S. Patel, H. Clevers, M. M. Taketo, F. Long, A.P. McMahon, R.A. Lang, G. Karsenty, Canonical Wnt signaling in differentiated osteoblasts controls osteoclast differentiation, Dev. Cell 8 (2005) 751–764.
[34] M. Kawai, S. Mushiake, K. Bessho, M. Murakami, N. Namba, C. Kokubu, T. Michigami, K. Ozono, Wnt/Lrp/beta-catenin signaling suppresses adipogenesis by inhibiting mutual activation of PPARgamma and C/EBPalpha, Biochem. Biophys. Res. Commun. 363 (2007) 276–282.
[35] D.W. Kang, C.Y. Choi, Y.H. Cho, H. Tian, G. Di Paolo, K.Y. Choi, S. Min do, Targeting phospholipase D1 attenuates intestinal tumorigenesis by controlling beta-catenin signaling in cancer-initiating cells, J. Exp. Med. 212 (2015) 1219–1237.
[36] H.I. Song, M.S. Yoon, PLD1 regulates adipogenic differentiation through mTOR - IRS-1 phosphorylation at serine 636/639, Sci. Rep. 6 (2016) 36968.
[37] Y.H. Lee, Y.S. Bae, Phospholipase D2 downregulation induces cellular senescence through a reactive oxygen species-p53-p21Cip1/WAF1 pathway, FEBS Lett. 588 (2014) 3251–3258.
[38] S. Khosla, Minireview: the OPG/RANKL/RANK system, Endocrinology 142 (2001) 5050–5055.
[39] P.L. Chung, S. Zhou, B. Eslami, L. Shen, M.S. LeBoff, J. Glowacki, Effect of age on regulation of human osteoclast differentiation, J. Cell. Biochem. 115 (2014) 1412–1419.

[40] Q. Chen, P. Shou, C. Zheng, M. Jiang, G. Cao, Q. Yang, J. Cao, N. Xie, T. Velletri, X. Zhang, C. Xu, L. Zhang, H. Yang, J. Hou, Y. Wang, Y. Shi, Fate decision of mesenchymal stem cells: adipocytes or osteoblasts? Cell Death Differ. 23 (2016) 1128–1139.

[41] C.N. Bennett, K.A. Longo, W.S. Wright, L.J. Suva, T.F. Lane, K.D. Hankenson, O. A. MacDougald, Regulation of osteoblastogenesis and bone mass by Wnt10b, Proc. Natl. Acad. Sci. U. S. A. 102 (2005) 3324–3329.

[42] J. Justesen, K. Stenderup, E.N. Ebbesen, L. Mosekilde, T. Steiniche, M. Kassem, Adipocyte tissue volume in bone marrow is increased with aging and in patients with osteoporosis, Biogerontology 2 (2001) 165–171.

[43] S. Verma, J.H. Rajaratnam, J. Denton, J.A. Hoyland, R.J. Byers, Adipocytic proportion of bone marrow is inversely related to bone formation in osteoporosis, J. Clin. Pathol. 55 (2002) 693–698.

[44] C.J. Rosen, M.L. Bouxsein, Mechanisms of disease: is osteoporosis the obesity of bone? Nat. Clin. Pract. Rheumatol. 2 (2006) 35–43.

[45] M. Herrmann, Marrow fat-secreted factors as biomarkers for osteoporosis, Curr Osteoporos Rep (2019).

[46] N. Kumashiro, D.M. Erion, D. Zhang, M. Kahn, S.A. Beddow, X. Chu, C.D. Still, G. S. Gerhard, X. Han, J. Dziura, K.F. Petersen, V.T. Samuel, G.I. Shulman, Cellular mechanism of insulin resistance in nonalcoholic fatty liver disease, Proc. Natl. Acad. Sci. U. S. A. 108 (2011) 16381–16385.